Clinical Neurophysiology 118 (2007) 918–927

www.elsevier.com/locate/clinph

Small-world networks and epilepsy: Graph theoretical analysis of intracerebrally recorded mesial temporal lobe seizures ☆

S.C. Ponten [a,*], F. Bartolomei [b], C.J. Stam [a]

[a] *Department of Clinical Neurophysiology, VU University Medical Centre, P.O. Box 7057, 1007 MB, Amsterdam, The Netherlands*
[b] *Service de Neurophysiologie Clinique, INSERM U 751, CHU TIMONE et Université de la Méditerranée, 13385 Marseille Cedex 5, France*

Accepted 5 December 2006

Abstract

Objective: Neuronal networks with a so-called 'small-world' topography (characterized by strong clustering in combination with short path lengths) are known to facilitate synchronization, and possibly seizure generation. We tested the hypothesis that real functional brain networks during seizures display small-world features, using intracerebral recordings of mesial temporal lobe seizures.
Methods: We used synchronization likelihood (SL) to characterize synchronization patterns in intracerebral EEG recordings of 7 patients for 5 periods of interest: interictal, before-, during- and after rapid discharges (in which the last two periods are ictal) and post-ictal. For each period, graphs (abstract network representations) were reconstructed from the synchronization matrix and characterized by a clustering coefficient C (measure of local connectedness) and a shortest path length L (measure of overall network integration). Results were also compared with those obtained from random networks.
Results: The neuronal network changed during seizure activity, with an increase of C and L most prominent in the alpha, theta and delta frequency bands during and after the seizure.
Conclusions: During seizures, the neuronal network moves in the direction of a more ordered configuration (higher C combined with a slightly, but significantly, higher L) compared to the more randomly organized interictal network, even after correcting for changes in synchronization strength.
Significance: Analysis of neuronal networks during seizures may provide insight into seizure genesis and development.

Keywords: Intracerebral EEG; "Small-world" networks; Synchronization; Temporal lobe epilepsy; Seizures; Graph theory

1. Introduction

Epilepsy is a common neurological disorder, characterized by sudden occurrence of unprovoked seizures (Hauser et al., 1993). The unforeseen and unpredictable way in which seizures occur is one of the most disabling aspects of epilepsy. The underlying pathophysiology of epileptic seizures is still poorly understood (Timofeev and Steriade, 2004). How and when the transition from an interictal to an ictal state takes place is not known. However, it is widely accepted that an abnormal synchronization of neurons is a part of seizure generation. Several findings indicate that the transition may not always occur abruptly, but may show a predisposing state called 'preictal' which can be characterized by either desynchronization or hypersynchronization (Mormann et al., 2003; Lopes da Silva et al., 2003; Le Van Quyen et al., 2005; Wendling et al., 2005).

Apart from changes in overall levels of synchronization the interictal–ictal transition may also be characterized by changes in the spatial organization of the involved networks. This can be studied with the use of 'graph theory'

Abbreviations: BRD, before rapid discharges ('preictal'); DRB, during rapid discharges; ARD, after rapid discharges.

☆ The analysis was performed in the VU University Medical Centre, but the SEEG registrations were performed in the Epilepsy Unit at Timone Hospital (Marseille, France).

* Corresponding author. Tel.: +31 20 4440730; fax: +31 20 4444816.
E-mail address: sc.ponten@vumc.nl (S.C. Ponten).

1388-2457/$32.00
doi:10.1016/j.clinph.2006.12.002

(see Fig. 1) (Strogatz, 2001; Wang and Chen, 2003; Boccaletti et al., 2006). Graphs are abstract representations of networks which can be characterized by a clustering coefficient (C) a measure for local connectedness and a characteristic path length (L) an indicator of overall integration. Watts and Strogatz (1998) showed that graphs with many local connections and a few random long distance connections (characterized by a high C and a short L) are near optimal networks, called 'small-world networks', which are intermediate between ordered (high C and long L) and random networks (low C and short L) (see Fig. 2). It has been shown that neuronal networks, like many other networks (e.g. the internet, the social network), show characteristic 'small-world' features (Strogatz, 2001). It is suggested that a small-world-like network may be optimal for synchronizing neuronal activity between different brain regions (Lago-Fernandez et al., 2000; Barahona and Pecora, 2002). Graph-analysis of anatomical and functional data such as fMRI, EEG and MEG showed a small-world configuration (Sporns et al., 2000; Stam, 2004; Salvador et al., 2005; Achard et al., 2006; Stam et al., 2007; Micheloyannis et al., 2006a; Micheloyannis et al., 2006b).

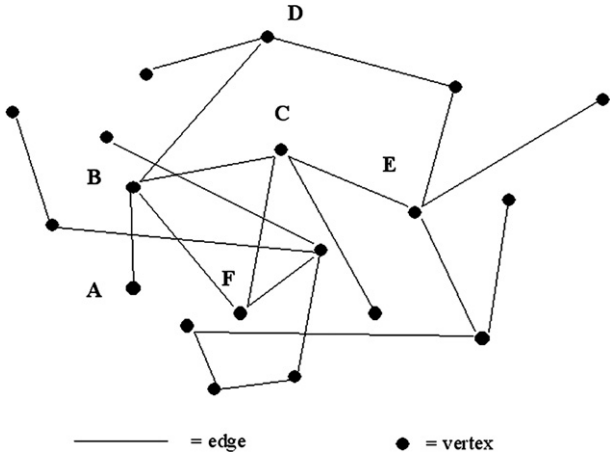

Fig. 1. This figure is based upon Stam et al. (2007). Schematic explanation of a graph and the graph theoretical measures. A graph consists of vertices, denoted by black dots. If two vertices are connected a line is drawn between them. This connection is called an edge. The size of the graph is the total number of vertices, in our study the EEG channels: $N = 21$. The degree k of a graph is the average number of edges per vertex. In a graph all vertices need to be connected. The smallest number of edges that have to be traveled to get from one vertex to the other expresses the distance between two vertices. For instance the shortest path from vertex A to vertex E has a length of 3 edges. The characteristic path length L of a graph is the mean of all shortest paths connecting all pairs of vertices. L is a measure of how well connected a graph is. To avoid the problem of the disconnected graphs we used an alternative approach based on the global efficiency (Latora and Marchiori, 2001) where L is calculated as the reciprocal of the average of the reciprocals. Infinite values of L (when two edges are not connected in the graph) contribute nothing to the sum (Newman, 2003). The clustering coefficient C is a measure of local structure. For example: to compute the clustering coefficient of vertex B, first determine the other vertices directly connected to vertex B (with path length 1). These neighbors are A, C, D and F. Then determine how many edges exist between this set of neighbors, in this example only 1 (the connection between C and F). Node B has 4 neighbors, which leads to 6 possible connections between these neighbors (k neighbors: k^* $(k-1)/2$ potential undirected edges). The clustering coefficient of B is the ratio of these two numbers: 1/6. In a similar way, the clustering coefficient can be determined of all vertices. This results in an average clustering coefficient C of the graph. Disconnected points are assigned a value of 0. The clustering coefficient is a measure of the existence of local clustering within a network.

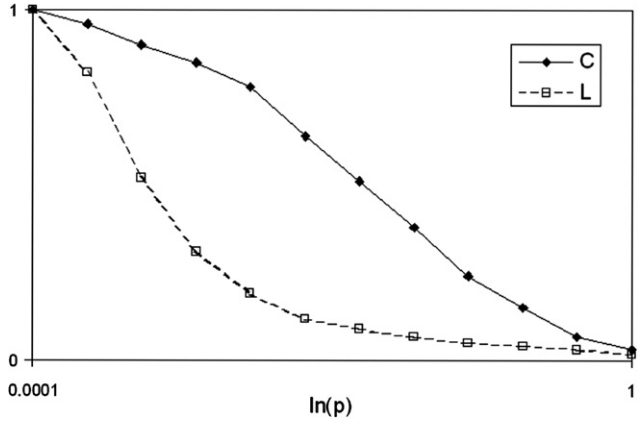

Fig. 2. Example of the clustering coefficient (C) and characteristic path length (L) as a function of the rewiring probability p. The rewiring probability is the probability that an edge between two vertices is randomly rewired. A totally ordered network has $p = 0$ and a random network $p = 1$ (all vertices are randomly connected). As shown in the figure for a small probability of rewiring (p close to zero) the local properties of the network are still the same as in the ordered network with an almost unchanged clustering coefficient C, whereas the path length L drops rapidly to the same order as random networks. Networks with this configuration (a high C and relative low L) are so called small-world networks. Note the logarithmic scale in the p-values at the x-axis. This figure is not based on real data.

Recently, a relationship between the small-world phenomenon and epilepsy was suggested by two model studies. Netoff et al. (2004) simulated a small-world network model of excitatory neurons to explain seizure dynamics in a hippocampal slice. They found that seizure activity corresponded with a small-world regimen of the neurons. Moreover, the start of the bursting phase corresponded with a drop of C, and thus a random instead of small-world architecture. Percha et al. (2005) showed a potential mechanism underlying seizure generation. They used a model with a two dimensional lattice of coupled neurons to show that properties of phase synchronization change radically depending on the connectivity structure of the network. In particular, a small-world configuration was associated with a low threshold for seizure generation.

Finally, both studies showed that a small-world and even more a random structure in models are associated with an increase in synchronization and probably with seizures. However, this has never been tested in seizure recordings in patients. We investigated the hypothesis that functional neuronal networks during temporal lobe seizures change in configuration before and during seizures, by applying synchronization and graph analysis to intracerebral EEG recordings. We studied graph configuration in 5 periods of interest: interictal, preceding, during (two) and

after the seizure. The characteristics of the periods around the seizure were compared with interictal EEG to investigate whether the neuronal network changes during the seizure and what the initial configuration is of the interictal network.

2. Materials and methods

2.1. Patient selection

Seven patients were selected from a group undergoing pre-surgical evaluation of drug-resistant mesial temporal lobe epilepsy (MTLE) (see Table 1 for patient characteristics). Data from these patients were previously reported in several studies (Bartolomei et al., 2001; Bartolomei et al., 2004; Bartolomei et al., 2005; Wendling et al., 2005). The patients we selected had seizures that involved the medial temporal lobe at onset and had comparable seizure patterns. All patients had a comprehensive evaluation including detailed history and neurological examination, neuropsychological testing, routine magnetic resonance imaging (MRI), surface electroencephalography (EEG) and stereoelectroencephalography (SEEG, depth electrodes). The latter was performed during long-term video-EEG monitoring in the Epilepsy Unit at Timone Hospital (Marseille, France). SEEG was carried out as part of our patients' normal clinical care. Informed consent was obtained from all patients.

2.2. EEG recording

SEEG recordings were performed using intracerebral multiple contact electrodes (10–15 contacts, length: 2 mm, diameter: 0.8 mm, 1.5 mm apart) placed intracranially according to Talairach's stereotactic method (Talairach et al., 1992). The original reference electrode is a scalp reference Pz. We used a scalp reference because the intracerebral signal is largely of higher amplitude than the surface one. Positioning of electrodes was established in each patient based upon available non-invasive information and hypotheses about the localization of the epileptogenic zone. Implantation accuracy was per-operatively controlled by telemetric X-ray imaging. A post-operative computerized tomography (CT) scan without contrast was used to verify absence of bleeding and precise location of each recording lead. Intracerebral electrodes were removed after the registration and a magnetic resonance imaging (MRI) was performed, permitting visualization of the trajectory of each electrode. Finally, CT-scan/MRI data fusion was performed to anatomically locate each contact along the electrode trajectory. Fig. 3a shows a typical scheme of SEEG orthogonal implantation of depth electrodes. All patients had electrodes that spatially sampled mesial/limbic regions (amygdala, entorhinal cortex and hippocampus) and lateral/neocortical regions of the temporal lobe. In addition, all selected patients had a varying number of electrodes that sampled the parietal cortex and the frontal lobe. In the present analysis we used 21 leads. Seven regions (amygdala, anterior, medial and posterior part of neocortex of the medial temporal gyrus, anterior and posterior hippocampus and the occipito-temporal sulcus) were represented in all recordings; the other regions were used variably. Signals were recorded on a 128 channels Deltamed™ system. They were sampled at 256 Hz and recorded on a hard disk (16 bits/sample) using no digital filter. The filters present in the acquisition procedure were a hardware analog high-pass filter (cut-off frequency equal to 0.16 Hz) used to remove very slow variations that sometimes contaminate the baseline and a first order low-pass filter (cut-off frequency equal to 97 Hz) to avoid aliasing.

2.3. EEG signal analysis

The signals recorded in each patient were first visually analyzed, and a typical seizure was selected. Besides a representative artifact free interictal epoch of 16 s, four epochs of interest were selected around the seizure. The selection criteria were also used in previous studies with the same population: before rapid discharge (BRD or before seizure onset), during rapid discharges (DRD, or early ictal), directly after rapid discharges, during seizure spreading

Table 1
Patient characteristics

Patients	1	2	3	4	5	6	7
Age (y)	30	35	14	38	36	36	35
Gender	M	M	F	F	F	M	F
Age at onset (y)	22	32	11	14	20	18	32
Etiology	HS	HS	HS	HS	HS	Unk	CD
MRI	Right HS left frontal arachnoidal cyst	Right HS	Left HS	Left HS	Right HS	normal	CD right MTL and thalamus
Type of TLE	R-MTLE	R-MTLE	L-MTLE	L-MTLE	R-MTLE	L-MTLE	R-MTLE
Type of surgery	ATL	ATL	ATL	ATL	ATL	NO	ATL
Follow-up (years)	4	3	3	3	2	–	2
Post-surgical outcome (ILAE)[a]	1	1	1	1	1	–	1

Abbreviations. L, left; R, right; HS, hippocampal sclerosis; MTLE, mesial temporal lobe epilepsy; ATL, anterior temporal lobectomy; Unk, unknown; CD, Taylor's cortical dysplasia.

[a] Post-surgical outcome according to the International league against epilepsy (ILAE) classification (Wieser et al., 2001).

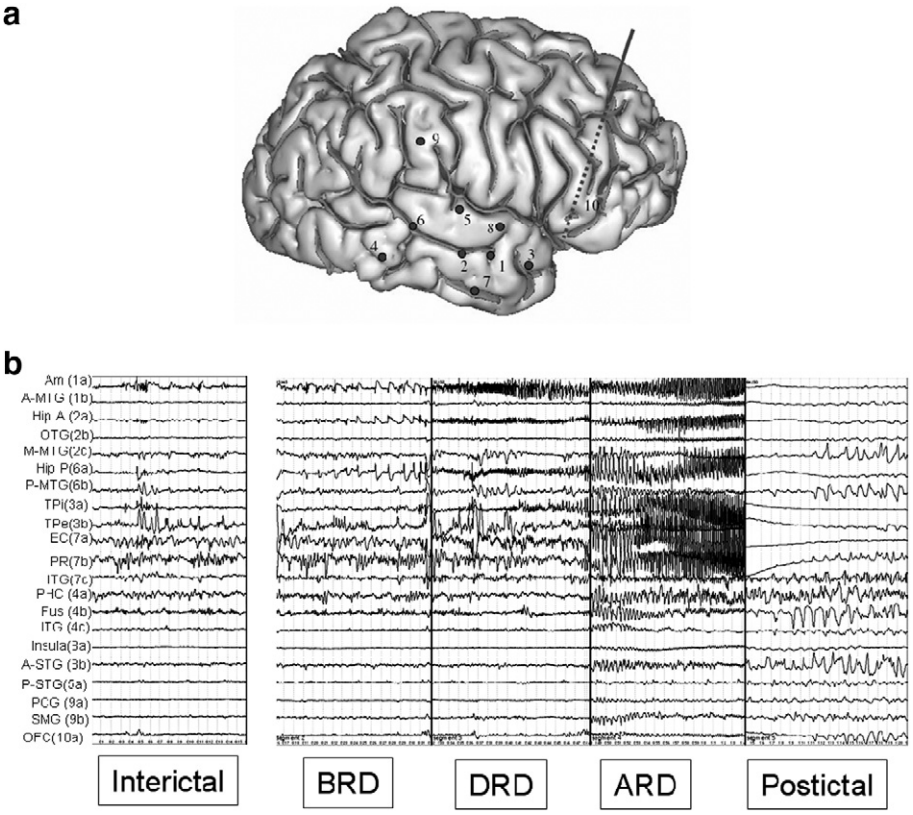

Fig. 3. (a) A schematic diagram of SEEG electrode placement on a lateral view of the Talairach's basic referential system (Talairach et al., 1992). (1) Electrode exploring the amygdala (internal leads, 1a) and the neocortical anterior part of the medial temporal gyrus (MTG) (external leads, 1b). (2) Electrode exploring the anterior hippocampus (internal leads, 2a), the occipito-temporal sulcus (middle leads, 2b) and the neocortical middle part of MTG (external leads, 2c). (3) Electrode exploring the internal part of the temporal pole (internal leads, 3a) and the external part of the temporal pole (external leads, 3b). (4) Electrode exploring the posterior parahippocampal region (internal leads, 4a), the fusiform gyrus (middle leads, 4b) and the posterior part of the temporobasal cortex (lateral contacts, 4c). (5) Electrode exploring the thalamus (internal leads, 5a), the insular lobe (middle leads, 5b) and the superior temporal gyrus (external leads, 5c). (6) Electrode exploring the posterior hippocampus (internal leads, 6a) and the posterior part of MTG (external leads, 6b). (7) Electrode exploring the entorhinal cortex (internal leads, 7a), the perirhinal cortex (middle leads, 7b) and the lateral temporobasal cortex (external leads, 7c). (9) Electrode exploring the posterior cingulate gyrus (internal leads, 9a) and the supramarginalis gyrus (middle leads, 9b). (10) Electrode exploring the orbitofrontal cortex (internal leads, 10a). Signals recorded by these electrodes were used in this study. We did not use electrode 8 in our calculations. (b) Example of intracerebral recording performed during SEEG and the corresponding studied periods. Five periods of 16 s each are chosen during interictal period, before the appearance of the rapid discharges within the medial structures (BRD), during the period of appearance of the rapid discharges (DRD), during the phase following the rapid discharges (ARD), corresponding to the spreading of the discharges beyond the mesial temporal structures and the postictal period.

(ARD, or late ictal) and postictal (Bartolomei et al., 2004; Wendling et al., 2005). An explanation about the epoch-selection is described elsewhere in detail (Bartolomei et al., 2004). Fig. 3b gives a clear example of different epochs selected in one of the patients (patient 3).

Bipolar signals from adjacent contacts of electrodes were selected in order to obtain the signals from 21 brain regions in each patient (see Fig. 3a). Besides the broad signal band (1–48 Hz), we analyzed digital, zero-phase shift filtered signals. The signal was digitally filtered in different frequency bands: delta (1–4 Hz), theta (4–8 Hz), alpha (8–13 Hz), beta (13–30 Hz) and gamma (30–48 Hz).

2.4. Computation of the synchronization likelihood (SL)

To calculate the characteristics of the network we used the synchronization likelihood (SL), a measure for statistical interdependencies between a time series (such as an EEG channel) and one or more other time series, within a dynamical system, introduced by Stam and van Dijk (2002). This measure has already been used in several studies of healthy subjects and patients (Stam et al., 2003; Posthuma et al., 2005; Stam et al., 2007; Bartolomei et al., 2006b). For a detailed explanation, see Appendix A. Here we give a brief description based upon Stam et al. (2007). The SL is sensitive to linear as well as to nonlinear interdependencies. Basic principle of the SL is to divide each time series into a series of 'patterns' and to search for a recurrence of these patterns. The SL is the chance that pattern recurrence in time series X coincides with pattern recurrence in time series Y. SL ranges between 1 in case of maximally synchronous signals and P_{ref} (a small number close to zero) in case of independent time series. P_{ref} is the small but non-zero likelihood of coincident pattern recurrence in case of independent time series. The end result of computing SL for all pair-wise combinations of channels is a

square $N \times N$ matrix of size 21 (21 is the number of EEG channels used in this study), where each entry $N_{i,j}$ contains the value of the SL for the channels i and j. We computed also the average synchronization by taking the mean of these values. This resulted in a single overall SL value for each epoch (16 s) studied.

2.5. Computation of the clustering coefficient C and the path length L

To compute the clustering coefficient C and characteristic path length L from the EEG data, we used the method described by Stam et al. (2007). The first step is to convert the synchronization $N \times N$ matrices into a binary graph, with N the number of EEG channels, using an individually adapted threshold T which resulted for all graphs in a value of $k = 6$. We start with a threshold of zero, and then count the number of connections (pairwise SL values) higher than the threshold. The degree k is the number of suprathreshold connections divided by the total number of connections. Then the threshold is increased (in very small steps) and the procedure is repeated. With increasing threshold the degree will decrease. The procedure is repeated until the required degree is reached. Only those SL values higher than the threshold will be considered edges; in the case of subthreshold SL there is no edge between the corresponding vertices. This procedure is repeated for each individual-analyzed epoch. To counteract the influence of synchronization differences among the epochs on C and L, we computed C and L as a function of a fixed k, which is the average number of edges per vertex. In this way, graphs in all epochs are guaranteed to have the same number of edges, so that any differences in C and L among the stages reflect differences in graph organization and will not be influenced by epoch differences in the mean strength of synchronization.

Once the graph has been made, the next step is to characterize this graph in terms of its clustering coefficient (C) and its characteristic path length (L). An explanation of these measures is given in Fig. 1. We choose not to use the conventional calculation of L, because this method does not deal properly with disconnected edges. Because this takes place in our data during and after the seizure, we found an alternative approach. Newman (2003) proposed to define L to be the 'harmonic mean' distance between pairs, or the reciprocal of the average of the reciprocals. In this way, calculation of L resembles the global efficiency introduced by Latora and Marchiori (2001). Afterwards the values of C and L were compared to theoretical values of random networks generated following the procedure described by Sporns and Zwi (2004) which preserve the degree distribution exactly. For a k value of 6 for each epoch 20 random networks were generated and the mean C-s and L-s of all these networks were calculated as reference value for C and L (C/C-s and L/L-s). These scaled values were used in further analysis.

Computation of the synchronization likelihood and of the two graph theoretical measures C and L was done with the DIGEEGXP software written by one of the authors (CS).

2.6. Statistical analysis

Statistical analysis consisted of Wilcoxon matched pairs tests to detect differences of synchronization likelihood, scaled clustering coefficient C/C-s and path length L/L-s among the interictal versus the other periods of interest before, during and after rapid discharges and postictal.

3. Results

3.1. Synchronization likelihood

Fig. 4 shows the mean synchronization likelihood (SL) for 5 epochs of interest (interictal, before rapid discharges (BRD), during rapid discharges (DRD), after rapid discharges (ARD) and postictal) through the seizure in broad band filtered signal (1–48 Hz) and filtered signals in separate frequency bands (1–4, 4–8, 8–13, 13–30 and 30–48 Hz). As can be seen the mean synchronization likelihood increased during the seizure in all frequency bands. For statistical analysis, we compared SL from the epochs of interest BRD, DRD, ARD and postictal with SL obtained from the interictal epoch which was used as reference state. In the ARD phase, during spreading of seizure, the increase of the SL was significant in all frequency bands ($p < 0.05$). The SL increase in the BRD period was only significant in the delta frequency filtered signal (1–4 Hz). The DRD increase of SL was significant in alpha (8–13 Hz), beta (13–30 Hz) and delta bands. The postictal increase in the SL was significant in all frequency bands.

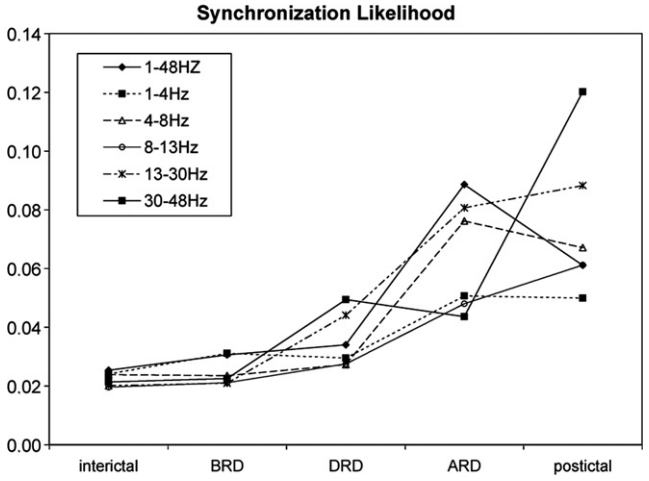

Fig. 4. Mean synchronization likelihood (SL) curves for all filtered frequency bands (delta 1–4 Hz, theta 4–8 Hz, alpha 8–13 Hz, beta 13–30 Hz and gamma 30–48 Hz) and the broad filtered signal (1–48 Hz). Each curve shows the changes in the different EEG epochs through seizure activity.

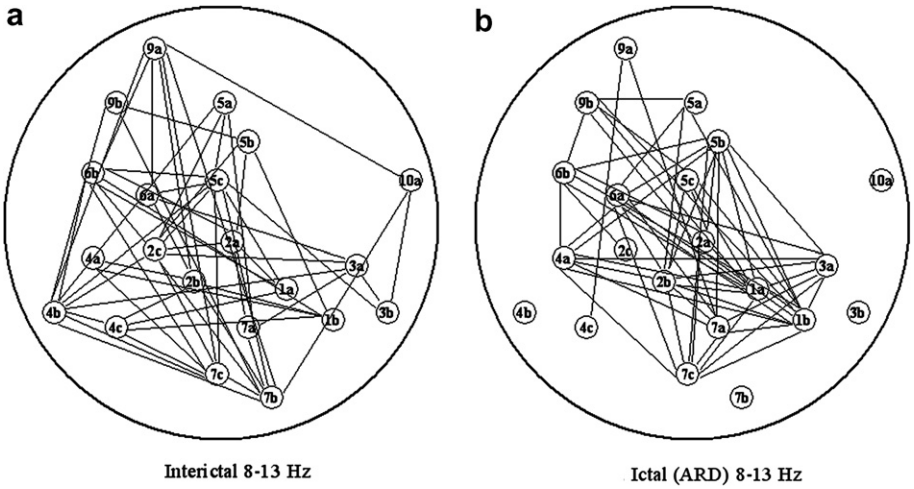

Fig. 5. Examples of graphs of patient 3, with the position of the electrodes indicated by small circles (see legend in Fig. 2). (a) is the interictal epoch. (b) is the after rapid discharges (ARD) epoch. For the conversion of the synchronization matrices to the graphs, $k = 3$ was used to show the difference of the configuration of the network. This means that the number of connections is guaranteed and that the strongest connections are counted and visualized in this picture.

3.2. Clustering coefficient C and characteristic path length L

The synchronization $N \times N$ matrices were converted to graphs, using an individual-adapted threshold T which resulted for all graphs in a value of $k = 6$. As an example Fig. 5 shows the graph of patient 3 in interictal (Fig. 5a) and ARD phase (Fig. 5b). To visualize differences between both networks, we used $k = 3$. Otherwise, too many connections were made and the differences disappear in lines. As shown in this figure, the organization of the neuronal network was different during seizure activity, compared to the interictal state. In the ARD phase, the neuronal network was more centered on the medial temporal gyrus (anterior and posterior part) as the interictal network, whereby more vertices (intracerebral electrodes) became disconnected from the graph ('missing connective points') (Bartolomei et al., 2006b). From this graphs C and L were determined as described in the 'Materials and methods' section. The values of C and L were compared with the values for random graphs, using the procedure described by Sporns and Zwi (2004) (C/C-s and L/L-s). In the randomization procedure, the degree distributions of the original networks were preserved. The mean L/L-s ratio in the different epochs was slightly above 1 whereas the mean C/C-s ratio was between 1.25 and 1.8 (see Fig. 6).

We compared the scaled values of C/C-s and L/Ls-s from the BRD, DRD, ARD and postictal network configurations with parameters of the interictal network configuration in the different frequency bands. In the broad frequency signal (1–48 Hz) there were no statistically significant differences of C/C-s, L/L-s were significantly higher in the ARD epoch compared to the interictal epoch. In the filtered frequency bands there were more significant differences, suggesting changes in the neuronal network topology during the seizure (see Table 2). In the delta band (1–4 Hz) C/C-s was significantly higher during both seizure epochs compared to the interictal period. L/L-s was significantly higher in the ARD period compared to the interictal period. In the theta band (4–8 Hz) the ARD and postictal epochs were significantly different from the interictal one: C/C-s was higher and L/L-s had increased in the ARD period. In the alpha band (8–13 Hz) C/C-s and L/L-s were significantly higher during both seizure epochs and postictally. In the beta (13–30 Hz) and gamma (30–48 Hz) bands, there were no significant differences among the characteristics of the network, interictal versus the other periods of interest. As in the other frequency bands, in beta and gamma bands C/C-s and L/L-s tended to increase during seizure activity. Overall the most obvious change was an increase of local clustering (C/C-s) during the seizures in the lower frequency bands (1–13 Hz), which continued in the postictal period and, with an increase of the path length (L/L-s) during the rapid discharges (alpha band), during seizure spreading (1–13 Hz) and after the seizures (alpha and theta bands).

4. Discussion

Graph theoretical analysis was used to test the hypothesis of a small-world structure of brain networks during seizures compared to interictal recordings. We found an increase of the clustering coefficient C in the lower frequency bands (1–13 Hz), and an increase of the path length L (alpha and theta bands) during and after the seizure compared to the interictal recordings. The increase of L/L-s was significant but rather small (<1,5) which is more compatible with a small-world than an ordered configuration.

The graph analysis was based upon matrices of synchronization between pairs of recording channels. We found an increase of the mean synchronization likelihood (SL) among the EEG signals during seizure activity compared to the interictal epoch (Fig. 4). The increase was significant

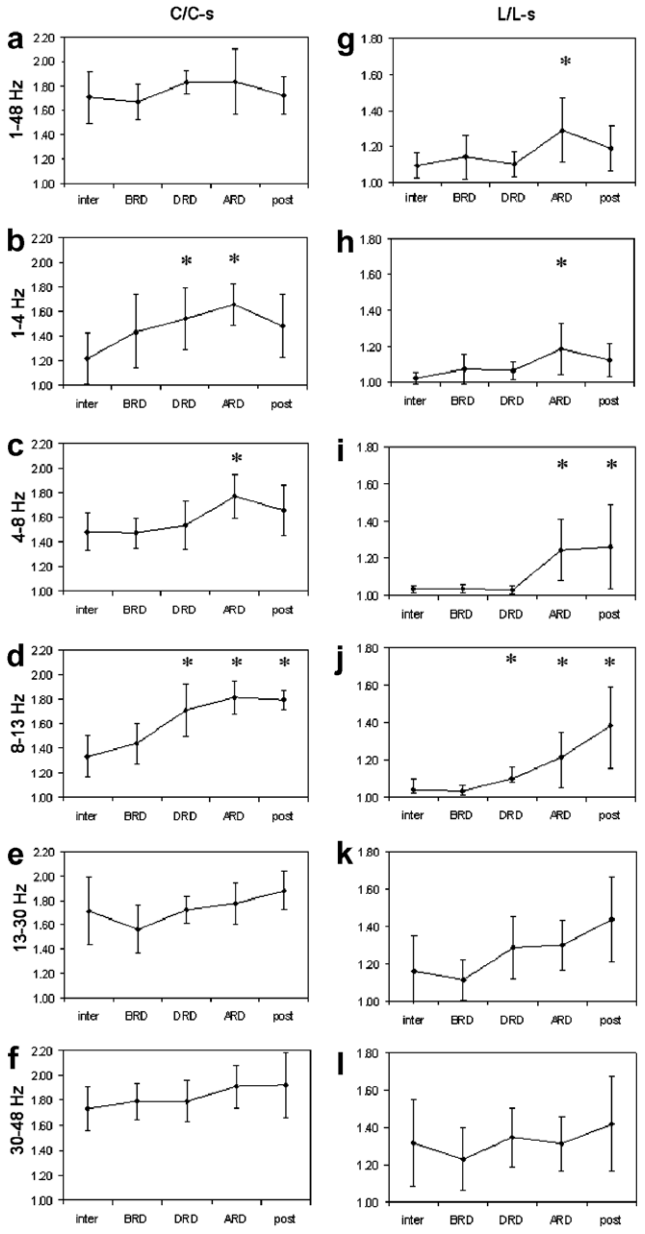

Fig. 6. (a–f) Mean scaled clustering coefficient C/C-s in the different frequency bands (a, 1–48 Hz; b, 1–4 Hz; c, 4–8 Hz; d, 8–13 Hz; e, 13–30 Hz; f, 30–48 Hz) and (g–l) scaled path length L/L-s in the different frequency bands (g, 1–48 Hz; h, 1–4 Hz; i, 4–8 Hz; j, 8–13 Hz; k, 13–30 Hz; l, 30–48 Hz) for all patients through the epochs of interest (interictal, BRD, DRD, ARD and postictal) with a fixed k. *significant ($p < 0.05$).

during seizure spreading (ARD) for all frequency bands, and for the alpha, beta and delta bands also during rapid discharges (DRD). Ferri et al. (2004) have shown the value of SL in seizure activity in their study of a nocturnal frontal lobe seizure. Although the seizure they used had another origin, they found a clear increase of SL in the alpha band (8–12 Hz) during seizure and in the delta band (0.5–4 Hz) at the end of the seizure. Zucconi et al. (2005) confirmed these results in three more patients with nocturnal frontal lobe seizures. In two patients there was involvement in multiple frequency bands. Besides, they showed a clear increase of SL a few seconds preceding the seizure. SL was able to pick up features of the EEG not evident in the visual analysis. Two other previous studies (Altenburg et al., 2003; Smit et al., 2004) demonstrated that SL in broad frequency bands seems to be a useful tool in epileptic seizure detection on the neonatal ward. The mean SL increased during seizure activity in neonatal EEG. Our study confirms the usefulness of SL in an approach to the dynamics of brain electrical synchronization in other types of seizures.

To test our main hypothesis topographical characteristics of the neuronal network were studied during the determined periods. Compared to the interictal period, we found an increase of scaled C (C/C-s) and L (L/L-s) during and after the seizure. The increase of C/C-s started in the alpha and delta bands during rapid discharges (DRD at seizure onset). During seizure spreading (ARD) there was an increase of C/C-s in all lower frequency bands (1–13 Hz), which continued postictally in the alpha band (see Table 2). The increase of L/L-s started at seizure onset (DRD) in the alpha band, continued during seizure spreading (ARD) in the lower frequency bands (1–13 Hz) and in the broad filtered signal, and lasted postictally in the alpha and theta bands. Since C/C-s and L/L-s increased significantly during seizure activity, it seemed that the interictal network had a more random configuration than the ictal one. In Fig. 2 the neuronal network moved to the left during the seizure, with an increase of C/C-s and L/L-s. Although the increase of L/L-s was significant, L/L-s did not exceed 1,5, which implied that the ictal neuronal network did not reach an ordered state (completely left in Fig. 2), rather a small-world configuration (somewhere in the middle region of Fig. 2).

During the seizures, the neuronal network changed from a more random network interictally, in the direction of a small-world structure. These findings are the first experimental proof of a more random architecture in a (less pathological) functioning network (the interictal state is by definition abnormal in these patients). Several studies have shown that anatomical neuronal networks display small-world characteristics (namely a high local clustering and also a short path length) (Strogatz, 2001). Stephan et al. (2000) showed that graph analysis can be applied equally well to patterns of functional and anatomical connectivity, in both cases a typical small-world network was revealed. In agreement with this, a few studies with fMRI and one with MEG data have shown typical small-world patterns in human brain networks (Stam, 2004; Salvador et al., 2005; Achard et al., 2006). In a recently published study with EEG data of Alzheimer patients and control subjects, Stam et al. (2007) also have shown a small-world pattern in healthy controls. In the Alzheimer patients the network showed a predominant loss of long-distance connections, resulting in a significantly longer L. Bartolomei et al. (2006a) have shown a randomization of the underlying neuronal network in MEG data of brain tumor patients compared to healthy controls. In the case of epilepsy the

Table 2
Results interictal epoch versus the other periods

p-values:	BRD		DRD		ARD		Postictal	
Frequency band (Hz)	*C*/*C*-s	*L*/*L*-s	*C*/*C*-s	*L*/*L*-s	*C*/*C*-s	*L*/*L*-s	*C*/*C*-s	*L*/*L*-s
1–48	–	–	–	–	–	.043	–	–
1–4	–	–	.043	–	.028	.046	–	–
4–8	–	–	–	–	.043	.018	–	.043
8–13	–	–	.018	.028	.018	.018	.018	.018
13–30	–	–	–	–	–	–	–	–
30–48	–	–	–	–	–	–	–	–

Abbreviations. BRD, before rapid discharges; DRD, during rapid discharges; ARD, after rapid discharges; *C*/*C*-s, clustering coefficient; *L*/*L*-s, path length. –, not significant.

situation seems to be different. In our study the small-world configuration was not associated with the less pathological state of the brain: the interictal state had less small-world features than the (late) ictal and postictal states. The interictal state seemed to function more as a random network than the (post)ictal condition. Whether this condition is an abnormal feature of the epileptic human brain is uncertain since there is no available study dealing with this problem. Chavez et al. (2006) suggested that random networks synchronize even better then small-world networks. In accordance with their statement it is possible that the interictal neuronal network structure in MTLE patients is not a normal, small-world-like network, but closer to a pathological random network which could lead to the onset of epileptic seizures. Following seizure onset, the neuronal network changes towards a more small-world configuration sustaining postictally. Percha et al. (2005) found that randomly connected networks have a dynamical regime of brain functioning where rapid phase transitions could take place and this state would correspond to seizure-like activity. The other previously published study about small-world networks and seizures Netoff et al. (2004) suggested also a relationship between small-world topography and seizure activity. They showed with a model of excitatory hippocampal neurons that networks with small-world features were more likely to generate seizures and randomly connected networks were associated with an even stronger tendency to synchronization (resulting in 'bursting' behavior). Although there are great differences in the data we used and the experimental studies, there are similarities that can be explored in future studies. There is one case study which applies graph-theoretical analysis at a seizure registered with depth electrodes (Wu et al., 2006). Their results, that the clustering coefficient increases during seizure activity, confirm our findings in seven patients.

Some considerations can be made about the method we used. Although we were able to show changes in the neuronal networks during seizures, even after a rigorous control for changes in synchronization strength, we should consider that the present analysis was done with large time-windows (16 s) and therefore gives a 'mean' but stable image of the network topography in each period. A more subtle analysis, using for example a sliding window, would be the next step to catch more dynamic and finer changes in the network dynamics. This method will make the comparison between the different seizure stages difficult and therefore we choose to compare relatively longer and more stabilized epochs for this first study. There are also some considerations with the application of graph theoretical analysis to EEG data. EEG signals record neuronal activity of virtual networks based on the correlation between EEG channels. This connectivity depends on, but is not the same as, the actual anatomical connections of the underlying neuronal network. Although there are suggestions in the literature that these networks are globally comparable (Kotter and Sommer, 2000). When transforming these data towards a graph, we measure the correlations between those channels and their brain areas but not the real anatomical network. Therefore it is important to correct for the different mean SL when calculating C and L, by fixing the mean number of connections per channel (k). When k is not kept constant in this calculation, C and L will be influenced more by the different synchronization instead of the changes of the underlying neuronal network (Stam et al., 2007).

This study is the first where small-world characteristics were studied in intracerebral EEG recordings of temporal lobe seizures. It provides support for changes in the direction of a more ordered configuration of functional brain networks during seizures. These changes were most prominent during seizure spreading. Interestingly, the postictal state also disclosed changes in network configuration. Furthermore, a more random configuration was found in the interictal recorded epochs which supported the theory of Netoff et al. (2004) and Chavez et al. (2006), that a random network even had a stronger tendency to synchronize. This suggests that the random interictal neuronal network configuration causes the seizures. This is the first step in what may become a promising research method to explore the dynamical processes underlying epilepsy. Future research should investigate whether patients suffering from mesial temporal lobe epilepsy have indeed particular random interictal state characteristics.

Acknowledgements

We thank Prof. dr P. Chauvel (Department of clinical neurophysiology, Marseille) for clinical and electrophysio-

logical assessment of the studied patients. We thank Prof. dr J. Régis (Neurosurgery department, Marseille) for the stereotactic placement of electrodes. Mrs E. van Deventer is thanked for her assistance with the literature search. This work was financially supported by the Dutch National Epilepsy Fund (NEF: Grant No. 05–12). We like to thank the three anonymous referees for their helpful comments on an earlier draft of this paper.

Appendix A. Mathematical background of synchronization likelihood

The synchronization likelihood (SL) is a measure of the *generalized synchronization* between two dynamical systems X and Y (Stam and van Dijk, 2002). Generalized synchronization (Rulkov et al., 1995) exists between X and Y of the state of the response system is a function of the driver system: $Y = F(X)$. The first step in the computation of the synchronization likelihood is to convert the time series x_i and y_i recorded from X and Y as a series of state space vectors using the method of time delay embedding (Takens, 1981):

$$X_i = (x_i, x_{i+L}, x_{i+2\times L}, x_{i+3\times L} \ldots, x_{i+(m-1)\times L}) \quad (1)$$

where L is the time lag, and m is the embedding dimension. From a time series of N samples, $N - (m \times L)$ vectors can be reconstructed. State space vectors Y_i are reconstructed in the same way.

Synchronization likelihood is defined as the conditional likelihood that the distance between Y_i and Y_j will be smaller than a cutoff distance r_y, given that the distance between X_i and X_j is smaller than a cutoff distance r_x. In the case of maximal synchronization this likelihood is 1; in the case of independent systems, it is a small, but nonzero, number, namely P_{ref}. This small number is the likelihood that two randomly chosen vectors Y (or X) will be closer than the cut-off distance r. In practice, the cut-off distance is chosen such that the likelihood of random vectors being close is fixed at P_{ref}, which is chosen the same for X and for Y. To understand how P_{ref} is used to fix r_x and r_y we first consider the correlation integral:

$$C_r = \frac{2}{N(N-w)} \sum_{i=1}^{N} \sum_{j=i+w}^{N-w} \theta(r - |X_i - X_j|) \quad (2)$$

Here the correlation integral C_r is the likelihood that two randomly chosen vectors X will be closer than r. The vertical bars represent the Euclidean distance between the vectors. N is the number of vectors, w is the Theiler correction for autocorrelation (Theiler, 1986) and θ is the Heaviside function: $\theta(X) = 0$ if $X >= 0$ and $\theta(X) = 1$ if $X < 0$. Now, r_x is chosen such that $\text{Cr}_x = P_{\text{ref}}$ and r_y is chosen such that $\text{Cr}_y = P_{\text{ref}}$. The synchronization likelihood between X and Y can now be formally defined as:

$$SL = \frac{2}{N(N-w)p_{ref}} \times \sum_{i=1}^{N} \sum_{j=i+w}^{N-w} \theta(r_x - |X_i - X_j|)\theta(r_y - |Y_i - Y_j|) \quad (3)$$

SL is a symmetric measure of the strength of synchronization between X and Y ($\text{SL}_{XY} = \text{SL}_{YX}$). In equation [3] the averaging is done over all i and j; by doing the averaging only over j SL can be computed as a function of time i. From [3] it can be seen that in the case of complete synchronization $\text{SL} = 1$; in the case of complete independence $\text{SL} = P_{\text{ref}}$. In the case of intermediate levels of synchronization $P_{\text{ref}} < \text{SL} < 1$. In the present study the following parameters were used: P_{ref} was set at 0.01, for the state space embedding a time lag of 10 samples, an embedding dimension of 10 and a Theiler correction (W2) of 0.1. When we tried the algorithm proposed by Montez et al. (2006), the results were comparable.

References

Achard S, Salvador R, Whitcher B, Suckling J, Bullmore E. A resilient, low-frequency, small-world human brain functional network with highly connected association cortical hubs. J Neurosci 2006;26(1):63–72.

Altenburg J, Vermeulen RJ, Strijers RL, Fetter WP, Stam CJ. Seizure detection in the neonatal EEG with synchronization likelihood. Clin Neurophysiol 2003;114(1):50–5.

Barahona M, Pecora LM. Synchronization in small-world systems. Phys Rev Lett 2002;89(5):054101.

Bartolomei F, Bosma I, Klein M, Baayen JC, Reijneveld JC, Postma TJ, et al. Disturbed functional connectivity in brain tumours patients: Evaluation by graph analysis of synchronization matrices. Clin Neurophysiol 2006a;117(9):2039–49.

Bartolomei F, Bosma I, Klein M, Baayen JC, Reijneveld JC, Postma TJ, et al. How do brain tumors alter functional connectivity? A magnetoencephalography study. Ann Neurol 2006b;59(1):128–38.

Bartolomei F, Khalil M, Wendling F, Sontheimer A, Regis J, Ranjeva JP, et al. Entorhinal cortex involvement in human mesial temporal lobe epilepsy: an electrophysiologic and volumetric study. Epilepsia 2005;46(5):677–87.

Bartolomei F, Wendling F, Bellanger JJ, Regis J, Chauvel P. Neural networks involving the medial temporal structures in temporal lobe epilepsy. Clin Neurophysiol 2001;112(9):1746–60.

Bartolomei F, Wendling F, Regis J, Gavaret M, Guye M, Chauvel P. Preictal synchronicity in limbic networks of mesial temporal lobe epilepsy. Epilepsy Res 2004;61(1–3):89–104.

Boccaletti S, Latora V, Moreno Y, Chavez M, Hwang DU. Complex networks: structure and dynamics. Phys Reports 2006;424(4–5):175–308.

Chavez M, Hwang DU, Amann A, Boccaletti S. Synchronizing weighted complex networks. Chaos 2006;16(1):015106.

Ferri R, Stam CJ, Lanuzza B, Cosentino FI, Elia M, Musumeci SA, et al. Different EEG frequency band synchronization during nocturnal frontal lobe seizures. Clin Neurophysiol 2004;115(5):1202–11.

Hauser WA, Annegers JF, Kurland LT. Incidence of epilepsy and unprovoked seizures in Rochester, Minnesota: 1935–1984. Epilepsia 1993;34(3):453–68.

Kotter R, Sommer FT. Global relationship between anatomical connectivity and activity propagation in the cerebral cortex. Philosophical transactions of the royal society of London series b-biological sciences 2000;355(1393):127–34.

Lago-Fernandez LF, Huerta R, Corbacho F, Siguenza JA. Fast response and temporal coherent oscillations in small-world networks. Phys Rev Lett 2000;84(12):2758–61.

Latora V, Marchiori M. Efficient behavior of small-world networks. Phys Rev Lett 2001;87(19):198701.

Le Van Quyen M, Soss J, Navarro V, Robertson R, Chavez M, Baulac M, et al. Preictal state identification by synchronization changes in long-term intracranial EEG recordings. Clin Neurophysiol 2005;116(3):559–68.

Lopes da Silva FH, Blanes W, Kalitzin SN, Parra J, Suffczynski P, Velis DN. Epilepsies as dynamical diseases of brain systems: basic models of the transition between normal and epileptic activity. Epilepsia 2003;44(Suppl 12):72–83.

Micheloyannis S, Pachou E, Stam CJ, Breakspear M, Bitsios P, Vourkas M, et al. Small-world networks and disturbed functional connectivity in schizophrenia. Schizophr Res 2006a;87(1–3):60–6.

Micheloyannis S, Pachou E, Stam CJ, Vourkas M, Erimaki S, Tsirka V. Using graph theoretical analysis of multi channel EEG to evaluate the neural efficiency hypothesis. Neurosci Lett 2006b;402(3):273–7.

Montez T, Linkenkaer-Hansen K, van Dijk BW, Stam CJ. Synchronization likelihood with explicit time-frequency priors. Neuroimage 2006;33(4):1117–25.

Mormann F, Kreuz T, Andrzejak RG, David P, Lehnertz K, Elger CE. Epileptic seizures are preceded by a decrease in synchronization. Epilepsy Res 2003;53(3):173–85.

Netoff TI, Clewley R, Arno S, Keck T, White JA. Epilepsy in small-world networks. J Neurosci 2004;24(37):8075–83.

Newman MEJ. The structure and function of complex networks. Siam Rev 2003;45(2):167–256.

Percha B, Dzakpasu R, Zochowski M, Parent J. Transition from local to global phase synchrony in small world neural network and its possible implications for epilepsy. Phys Rev E Stat Nonlin Soft Matter Phys 2005;72(3 Pt 1):031909.

Posthuma D, de Geus EJC, Mulder EJCM, Smit DJA, Boomsma DI, Stam CJ. Genetic components of functional connectivity in the brain: the heritability of synchronization likelihood. Human Brain Mapp 2005;26(3):191–8.

Rulkov NF, Sushchik MM, Tsimring LS, Abarbanel HD. Generalized synchronization of chaos in directionally coupled chaotic systems. Phys Rev E Stat Phys Plasmas Fluids Relat Interdiscip Topics 1995;51(2):980–94.

Salvador R, Suckling J, Coleman MR, Pickard JD, Menon D, Bullmore E. Neurophysiological architecture of functional magnetic resonance images of human brain. Cereb Cortex 2005;15(9):1332–42.

Smit LS, Vermeulen RJ, Fetter WP, Strijers RL, Stam CJ. Neonatal seizure monitoring using non-linear EEG analysis. Neuropediatrics 2004;35(6):329–35.

Sporns O, Zwi JD. The small world of the cerebral cortex. Neuroinformatics 2004;2(2):145–62.

Sporns O, Tononi G, Edelman GM. Connectivity and complexity: the relationship between neuroanatomy and brain dynamics. Neural Netw 2000;13(8–9):909–22.

Stam CJ. Functional connectivity patterns of human magnetoencephalographic recordings: a 'small-world' network? Neurosci Lett 2004;355(1–2):25–8.

Stam CJ, van Dijk BW. Synchronization likelihood: an unbiased measure of generalized synchronization in mulitvariate data sets. Physica D 2002;163:236–51.

Stam CJ, Breakspear M, van Cappellen van Walsum AM, van Dijk BW. Nonlinear synchronization in EEG and whole-head MEG recordings of healthy subjects. Hum Brain Mapp 2003;19(2):63–78.

Stam CJ, Jones BF, Nolte G, Breakspear M, Scheltens P. Small-World Networks and Functional Connectivity in Alzheimer's Disease. Cereb Cortex 2007;17(1):92–9.

Stephan KE, Hilgetag CC, Burns GA, O'Neill MA, Young MP, Kotter R. Computational analysis of functional connectivity between areas of primate cerebral cortex. Philos Trans R Soc Lond B Biol Sci 2000;355(1393):111–26.

Strogatz SH. Exploring complex networks. Nature 2001;410(6825):268–76.

Takens F. Detecting strange attractors in turbulence. Lecture in mathematics 1981(898):366–81.

Talairach J, Bancaud J, Bonis A, Szikla G, Trottier S, Vignal JP, et al. Surgical therapy for frontal epilepsies. Adv Neurol 1992;57:707–32.

Theiler J. Spurious dimension from correlation algorithms applied to limited time-series data. Phys Rev A 1986;34(3):2427–32.

Timofeev I, Steriade M. Neocortical seizures: initiation, development and cessation. Neuroscience 2004;123(2):299–336.

Wang XF, Chen G. Complex networks: small-world, scale-free and beyond. IEEE Circuits Sys Mag. 2003:6–20.

Watts DJ, Strogatz SH. Collective dynamics of 'small-world' networks. Nature 1998;393(6684):440–2.

Wendling F, Hernandez A, Bellanger JJ, Chauvel P, Bartolomei F. Interictal to ictal transition in human temporal lobe epilepsy: insights from a computational model of intracerebral EEG. J Clin Neurophysiol 2005;22(5):343–56.

Wieser HG, Blume WT, Fish D, Goldensohn E, Hufnagel A, King D, et al. ILAE commission report. Proposal for a new classification of outcome with respect to epileptic seizures following epilepsy surgery. Epilepsia 2001;42(2):282–6.

Wu HH, Li XL, Guan XP. Networking property during epileptic seizure with multi-channel EEG recordings. 2006.

Zucconi M, Manconi M, Bizzozero D, Rundo F, Stam CJ, Ferini-Strambi L, et al. EEG synchronisation during sleep-related epileptic seizures as a new tool to discriminate confusional arousals from paroxysmal arousals: preliminary findings. Neurol Sci 2005;26(Suppl 3):s199–204.